

See discussions, stats, and author profiles for this publication at: <https://www.researchgate.net/publication/233744353>

New Insight into the Atomic Structure of Electrochemically Delithiated O₃-Li(1-x)CoO₂ (0 <= x <= 0.5) Nanoparticles

ARTICLE in NANO LETTERS · NOVEMBER 2012

Impact Factor: 13.59 · DOI: 10.1021/nl303036e · Source: PubMed

CITATIONS

26

READS

192

14 AUTHORS, INCLUDING:



Zelang Jian

University of Houston

30 PUBLICATIONS 603 CITATIONS

[SEE PROFILE](#)



Hong Li

Chinese Academy of Sciences

277 PUBLICATIONS 10,733 CITATIONS

[SEE PROFILE](#)



Zhaoxiang Wang

Chinese Academy of Sciences

166 PUBLICATIONS 5,470 CITATIONS

[SEE PROFILE](#)



Yuichi Ikuhara

The University of Tokyo

481 PUBLICATIONS 5,975 CITATIONS

[SEE PROFILE](#)

New Insight into the Atomic Structure of Electrochemically Delithiated $O_3\text{-Li}_{(1-x)}\text{CoO}_2$ ($0 \leq x \leq 0.5$) Nanoparticles

Xia Lu,^{†,§} Yang Sun,^{†,§} Zelang Jian,^{†,‡,§} Xiaoqing He,[†] Lin Gu,^{*,†} Yong-Sheng Hu,^{*,†,¶} Hong Li,[†] Zhaoxiang Wang,[†] Wen Chen,[†] Xiaofeng Duan,[†] Liquan Chen,^{†,¶} Joachim Maier,[§] Susumu Tsukimoto,^{||} and Yuichi Ikuhara^{||,⊥,#}

[†]Beijing National Laboratory for Condensed Matter Physics, Institute of Physics, Chinese Academy of Sciences, Beijing 100190, China

[‡]State Key Laboratory of Advanced Technology for Materials Synthesis and Processing, School of Materials Science and Engineering, Wuhan University of Technology, Wuhan 430070, China

[§]Max Planck Institute for Solid State Research, Stuttgart 70569, Germany

[¶]WPI Advanced Institute for Materials Research, Tohoku University, Sendai 980-8577, Japan

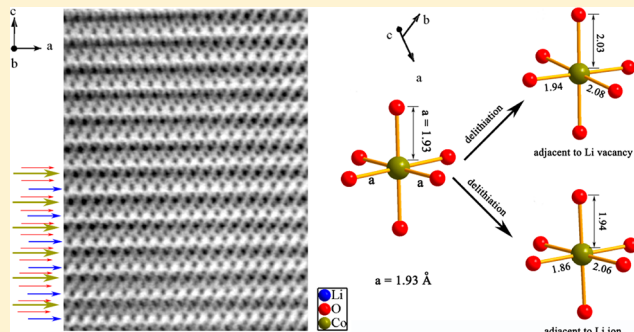
^{||}Nanostructures Research Laboratory, Japan Fine Ceramic Centre, Nagoya 456-8587, Japan

[#]Institute of Engineering Innovation, The University of Tokyo, Tokyo 113-8654, Japan

[⊥]School of Materials Science and Engineering, Chonnam National University, Gwangju 500-757, Republic of Korea

Supporting Information

ABSTRACT: Direct observation of delithiated structures of LiCoO_2 at atomic scale has been achieved using spherical aberration-corrected scanning transmission electron microscopy (STEM) with high-angle annular-dark-field (HAADF) and annular-bright-field (ABF) techniques. The ordered Li, Co, and O columns for LiCoO_2 nanoparticles are clearly identified in ABF micrographs. Upon the Li ions extraction from LiCoO_2 , the Co-contained (003) planes distort from the bulk to the surface region and the *c*-axis is expanded significantly. Ordering of lithium ions and lithium vacancies has been observed directly and explained by first-principles simulation. On the basis of HAADF micrographs, it is found that the phase irreversibly changes from O_3 -type in pristine LiCoO_2 to O_1 -type Li_xCoO_2 ($x \approx 0.50$) after the first electrochemical Li extraction and back to O_2 -type Li_xCoO_2 ($x \approx 0.93$) rather than to O_3 -stacking after the first electrochemical lithiation. This is the first report of finding $O_2\text{-Li}_x\text{CoO}_2$ in the phase diagram of $O_3\text{-LiCoO}_2$, through which the two previously separated LiCoO_2 phases, i.e. O_2 and O_3 systems, are connected. These new investigations shed new insight into the lithium storage mechanism in this important cathode material for Li-ion batteries.



KEYWORDS: LiCoO_2 , structural evolution, scanning transmission electron microscopy (STEM), Li-ion batteries

L $i\text{CoO}_2$, one of the most important cathode materials, has, with a great success, been commercially used in Li-ion batteries to power the smart mobile electrode devices and (hybrid) electric vehicles (EVs).^{1,2} Of its various structures, it is one thermodynamically stable O_3 -type LiCoO_2 (O in ABC stacking) which is usually obtained in the synthesis process, characterized by a space group $R\bar{3}m$ and lattice constants $a = 2.816 \text{ \AA}$ and $c = 14.080 \text{ \AA}$.¹ Contrarily, the O_2 -type LiCoO_2 (O in ABAC stacking), which is metastable and was prepared for the first time by Delmas et al. via Na^+/Li^+ exchange from the $\text{P}2\text{-Na}_{0.70}\text{CoO}_2$ phase, crystallizes in space group $P6_3mc$ with $a = 2.806 \pm 0.004 \text{ \AA}$ and $c = 9.52 \pm 0.01 \text{ \AA}$.^{3,4} Crystallographically, the lithium ions are located between two Co–O octahedron slabs along the [001] direction. In an electrochemical charging (delithiation)/discharging (lithiation) cycle,

different phases can be formed at through corresponding rearrangements of Co and O arrays along the [001] direction.^{5–18} The phase diagram was systematically studied, and a variety of phases, such as the O_3 , O_1 , $H1\text{--}3$ phases for O_3 -type LiCoO_2 ^{6–12} and O_2 , $T^{#2}$, $T^{#2'}$, O_6 phases for O_2 -type LiCoO_2 ,^{13–16} have been reported. It is obvious that all the phase transitions are strongly related to rearrangements of lithium ions and lithium vacancies.

According to previous studies, the layered $O_3\text{-Li}_x\text{CoO}_2$ ($0 \leq x \leq 1$) electrode exhibits complex phases upon Li extraction: (i) a solid-solution behavior is indicated in the charge curve

Received: August 15, 2012

Revised: November 5, 2012

Published: November 21, 2012

with minor Li extraction from the nanosized LiCoO_2 host;^{6,7,38} (ii) a first-order phase transition from an insulating $\text{Li}_{0.94}\text{CoO}_2$ phase to a metallic $\text{Li}_{0.75}\text{CoO}_2$ phase involving a significant expansion of the c -lattice parameter of the hexagonal cell occurs for $0.75 \leq x \leq 0.93$ as confirmed by *in situ* X-ray diffraction,^{6,7,17} by NMR results,¹⁹ and by first-principles calculation;²⁰ (iii) the O₃ structure and metallic characteristic are still kept in $0.50 < x \leq 0.75$;^{6,7,11} (iv) a phase transition from a rhombohedral lattice to monoclinic lattice at $x \approx 0.5$ of Li_xCoO_2 ;^{6,7,10} (v) a series of phase transitions, including H1–3 + O₃, H1–3, and H1–3 + O₁ phases, were reported upon Li extraction when $0 \leq x < 0.50$.^{9,16} Although Reimers et al. attributed the phase transition to order/disorder arrangements of lithium ions and lithium vacancies in (001) planes,⁶ Shao-Horn et al. identified the ordered/disordered arrangements of lithium ions and lithium vacancies along the [001] direction (staging phenomenon on lithium ion arrangement) by electron diffraction.¹⁰ The different ordered/disordered arrangements of lithium occupations and lithium vacancies have been simulated by first-principles calculation.⁹ However, it is of great difficulty to provide experimental evidence for the phase transitions and lithium occupation/vacancy ordering.

A solid-solution reaction with a reversible 0.5 mol Li insertion/extraction into/from O₃- LiCoO_2 is generally accepted in the early studies.^{6,7} Upon delithiation from LiCoO_2 to $\text{Li}_{0.5}\text{CoO}_2$, microscopic rearrangements and local chemical environment changes of Co and O ions occur. However, such detailed structural features are hard to address by diffraction techniques.

The visualization of Li ions in LiCoO_2 using high-resolution transmission electron microscopy was first achieved in ref 21 and then more clearly by the spherical-aberration-corrected scanning transmission electron microscopy (STEM) technique in ref 22. STEM techniques, with spatial resolution of ca. 0.40 Å, have been proved to be powerful tools in determining the fine structure in Li-ion battery system,^{22–33} such as visualization of the Li storage site (Li radius: 0.68 Å) and investigation of the local structure and surface/interface structures, which are beyond the capability of the bulk probing techniques, such as X-ray diffraction (XRD). Nevertheless, there are still some limitations of fully reflecting the structural change of the whole sample, which requires combination with other technique such as XRD. In this paper, the STEM technique and first-principles calculation are employed to investigate the structural evolutions in nanosized O₃- $\text{Li}_{(1-x)}\text{CoO}_2$ ($0 \leq x \leq 0.5$) cathode, including (i) arrangements of the Li ions and Li vacancies, (ii) distortion of the structure, and (iii) phase transitions.

The refinement XRD pattern of as-prepared LiCoO_2 sample fits very well with α -NaFeO₂ type structure ($\bar{R}\bar{3}m$), and the lattice constants are $a = 2.821$ Å and $c = 14.083$ Å (Figure S1). The $I_{(003)}/I_{(104)}$ of the sample is 1.30, the c/a ratio is equal to 4.99, and a clear split of (018)/(110) peak can be seen, indicating high crystallinity with very few antisites concerns Li and Co ions.³⁴ The particle size of the LiCoO_2 sample is ca. 500 Å in diameter from SEM image, and the lattice stripe distance in the TEM image is measured as 4.7 Å, corresponding to the LiCoO_2 (003) plane (Figure S2a–c). High crystallinity and the structure information are also confirmed by selected-area electron diffraction (SAED) (Figure S2d).

Figure 1 shows high-angle annular-dark-field (HAADF) and annular-bright-field (ABF) STEM micrographs of LiCoO_2 . Note that the contrast of the HAADF image varies with atomic number according to a $Z^{1/7}$ dependency in contrast to the ABF

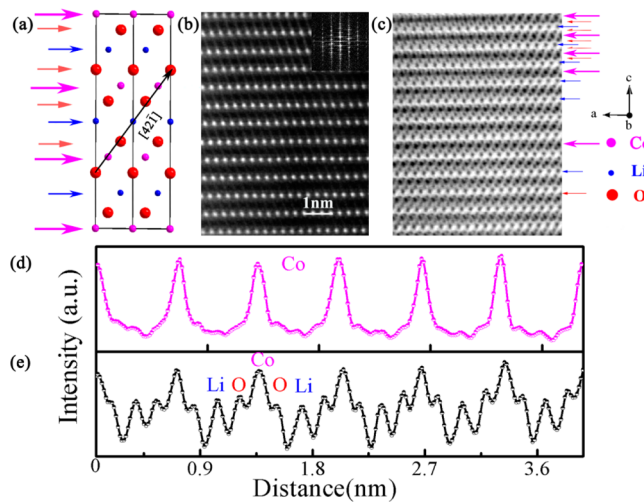


Figure 1. (a) Lattice structure, (b) HAADF with fast Fourier transformation (FFT) pattern inset, and (c) ABF STEM images of LiCoO_2 nanoparticles at the [010] zone axis. The corresponding line profiles of Co in HAADF image (d) and Li, Co, and O in ABF image (e) along the [42̄1] direction. In the ABF line profile, image contrast of the dark dots is inverted and displayed as peaks.

technique showing a $Z^{1/3}$ relationship.^{35,36} As far as the atomic-scale LiCoO_2 structure is concerned, Figure 1 displays the image of highest quality until now (see simulated images in Figure S3). Because the HAADF technique is more sensitive to the heavy atoms, Co ions are clearly seen from the HAADF image in Figure 1b. Figure 1d shows the homogeneous line contrast profiles of Co columns along [42̄1] direction projected at the [010] zone axis. The fast Fourier transformation (FFT) pattern of the inset in Figure 1b is also in accordance with the SAED in Figure S2d.

Concerning ABF micrographs, light elements (e.g., Li^{29,30}) can be distinguished at the proper zone axis. Besides the Co ions, Figure 1c unambiguously displays the Li and O columns. The 3b site Li ion columns, 3a site Co ion columns, and 6c site O ion columns are clearly identified with STEM-ABF techniques. The absence of abnormal contrast of Li, Co, and O in Figure 1e indicates the absence of Li–Co antisites (also see the simulated Li–Co antisites STEM images in Figure S3c,d and ref 37). Figure S4 shows the charge/discharge and differential capacity curves with an obvious redox peak at ca. 3.9 V in the LiCoO_2 first cycle. For *ex situ* STEM investigations, four samples, including (1) pristine, (2) ca. 0.25 mol of Li extracted, (3) ca. 0.50 mol of Li extracted, and (4) back to 3.0 V (ca. 0.43 mol of Li reinserted), were prepared for observations.

Among the STEM images, a remarkable distortion of the Co plane (003) near the surface regions is shown in Figure 2 (see raw pictures in Figure S5). In Figure 2a, kinks are present with regular directions while the local irregular distortions are found in Figure 2b,c. The distorted yellow dotted lines (Co plane) indicate an energetically favorable way to the release of interior stress to lower the bulk energy, which should be associated with the O array adjustments upon Li extraction.

With the Li ion extraction/insertion (relaxation of plane (003)), a larger planar distance of 0–0.3 Å in the surface region is commonly observed in the four STEM samples, which also implies movements of the Co–O octahedra (see the simulated results in Figures S6–S10). On the other hand, Figure 2d demonstrates the interior (003) planar distance at different Li

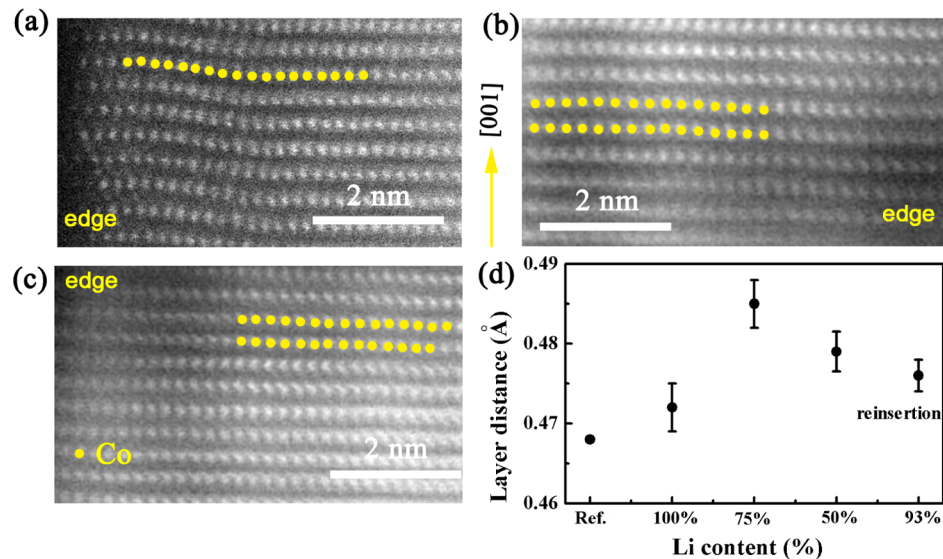


Figure 2. HAADF STEM images of LiCoO_2 electrode at [010] zone axis when (a) ca. 0.25 mol of Li extraction, (b) ca. 0.50 mol of Li extraction, and (c) back to 3.0 V (ca. 0.43 mol of Li reinsertion). (d) The planar distances of plane (003) in different Li contents including the value reported elsewhere; the yellow dots are labeled to guide the eyes. The planar distance is obtained by an average of the total length of several bulk layers (usual 10 layers).

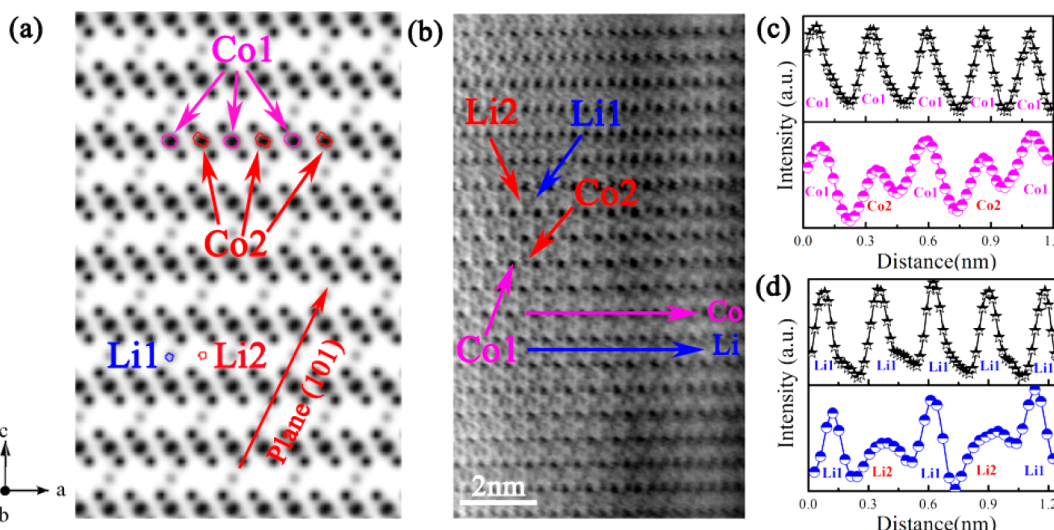


Figure 3. (a) Simulated ABF micrographic of O1-type $\text{Li}_{0.5}\text{CoO}_2$ with ordered Li occupancies/vacancies arrangements (Figure S6) at [010] zone axis. (b) STEM ABF image of LiCoO_2 electrode charged to 4.5 V at [010] zone axis. The corresponding line profiles of (c) Co columns and (d) Li columns in HAADF image, where the black line (☆) was acquired from the pristine LiCoO_2 ABF micrograph. In the ABF line profile, image contrast of the dark dots is inverted and displayed as peaks.

contents measured from the STEM images. Note that LiCoO_2 exhibits *c*-axis expansion during the Li ion extraction, experimentally from 4.72 Å (pristine) to 4.85 Å (ca. 0.25 Li extracted) and then to 4.79 Å (ca. 0.50 Li extracted). However, a little larger distance of 4.76 Å than that in the pristine (4.72 Å) (ca. 0.43 Li reinserted) was observed when the electrode is discharged to 3.0 V. This variation trend in *c*-axis is consistent with previous reports on the *in situ* XRD investigations where the interlayer distance along [001] direction is first broadened and then become smaller (still larger than that of pristine) in the Li extraction process.^{6,10} Feasible explanations for the expansion were net Coulombic repulsion of the opposite Co–O octahedra along [001] direction and Li ion occupancy/vacancy ordered/disordered distributions at the different Li contents, which means that the Li vacancy might arrange in a

disordered way in Li_xCoO_2 ($0.5 < x < 1$) host whereas the Li and Li vacancy are apt to occupying in an ordered way in $\text{Li}_{0.5}\text{CoO}_2$ host.

When the LiCoO_2 electrode was charged to 4.5 V (ca. 0.52 mol of Li extracted) in Figure 3b, the O3- LiCoO_2 has already transformed to the O1- LiCoO_2 according to the Co columns arrangements (see schematic view in Figure S11b). In Figure 3b,c, contrast of Co columns (pink line: ○) is obviously different from the black line (☆) acquired from the pristine LiCoO_2 ABF micrograph. The Co columns can be labeled as Co1 and Co2 columns, indicating different chemical environments (local site shift and/or the charge redistributions) of Co ion in the Co-containing (003) plane after Li ion extraction at such high voltage (see Figure S12). In Figure 3d, the Li ion columns (Li1 and Li2) in the blue line (○) are also found

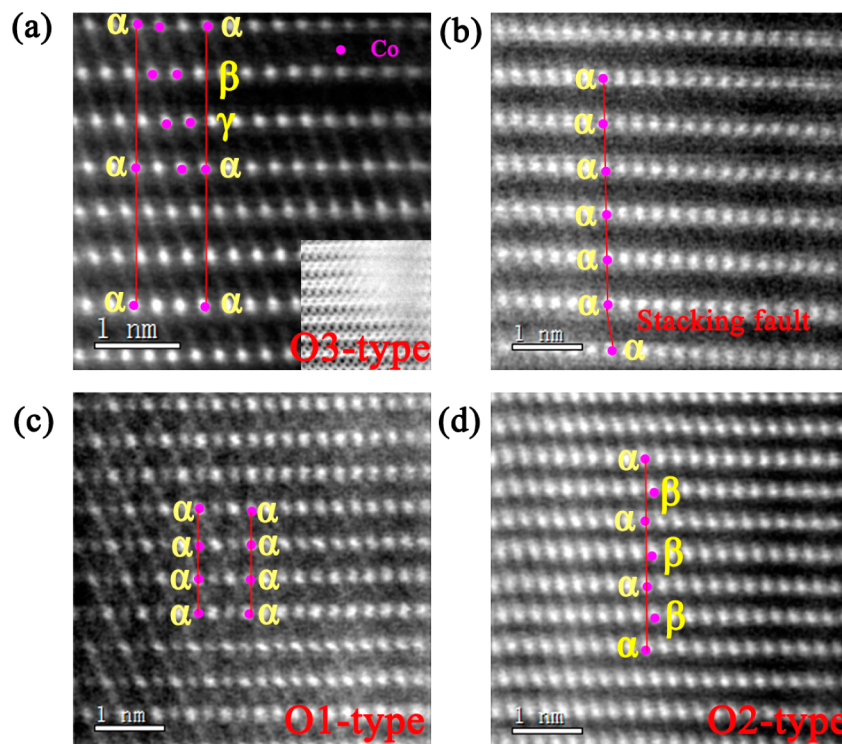


Figure 4. STEM HAADF image of surface structure (a) pristine LiCoO_2 , (b) LiCoO_2 charged to 4.2 V (full raw pictures with outmost layers are shown in Figure S13), (c) charged to 4.5 V, and (d) discharged to 3.0 V at the [010] zone axis.

different from the pristine material in the black line (\star). The Li ion columns show periodical arrangements, which are similar to the Li occupancy/vacancy arrangement in Figure 3a. Based on the different contrast of the columns in Figure 3a,b,d, a possible ordered Li ion occupancy/vacancy arrangement was observed along (101) plane (or other equivalent planes) in the O3-LiCoO₂ lattice. It shows that Li ions occupy every other (101) plane to form a staging-like ordered structure upon O3-LiCoO₂ host charged to 4.5 V (ca. 0.52 mol of Li extracted), as schematically illustrated in Figure 3a.

The different contrast of Co columns in Co-contained (003) plane should be ascribed to its interaction with the nearest Li ion and vacancy. Upon Li ion extraction, the initial Co^{3+} (low spin) ions are expected to be oxidized to Co^{4+} ions. The Co–O bond length in one Co–O octahedron changes by losing one electron (see the bond length changes in Figure S6). From first-principles calculations, one Co ion approaches to the Li vacancy and the spin state also changes from the low spin states to an intermediate high spin state, which might be related to the different contrast of the different Co columns in Figure 3b. It should be noted that, in the simulated ABF image (Figure 3a), the contrast based largely on the atomic position cannot totally represent the contrast difference between Co1 and Co2, which reflects the information on electron distributions and the distortions after Li extraction.

The phase transitions seem even more complex than observed in refs 11 and 19. The changes occur not only in the bulk but also on the outmost surface. Figure 4 gives an overview of the near surface configurations in the first cycle (see raw HAADF images with clear surface in Figure S13). The ordered Li, Co, and O columns extend to the outmost layer in O3-LiCoO₂ with a Co ion $\alpha\beta\gamma\alpha\beta\gamma$ -stack model in Figure 4a (O in ABCABC-stack model in Figure S11a). When this O3-LiCoO₂ was charged to 4.2 V (ca. 0.5 Li extracted), the Co

columns demonstrate the $\alpha\alpha\alpha$ -stack model in Figure 4b (O in ABAB-stack model in Figure S11b). This Co $\alpha\alpha\alpha$ -stack model corresponds to stacking-faulted O1-LiCoO₂. Interestingly, the phase transition from the previous phase to O1 type was observed at $x \approx 0.5$ in this nanosized Li_xCoO_2 . However, the O1 phase is regarded to be more stable when completely delithiated ($x \approx 0$).^{9,11} (Note that this transformation is unexpected according to the presently known phase diagram of LiCoO_2 , wherein the O3 phase is kept before $x = 0.5$ and O1 phase is not found until $x = 0.3$).^{9,11,12}) From Figure 4b, the planar distance in the surface region was obviously larger than in the pristine O3-LiCoO₂, with some stacking faults to buffer the uncompleted phase transition. When the sample is further charged to 4.5 V, the Co ions in Li_xCoO_2 display a regular $\alpha\alpha\alpha$ -stack model (O1-LiCoO₂ in Figure S11b) without stacking fault, indicating complete phase transition to O1-LiCoO₂. Furthermore, two different Co states as demonstrated in Figure 3 are confirmed again. These phenomena indicate that charging to a high voltage (i.e., 4.5 V) is the main driving force to obtain an ordered Li/vacancy distribution in about half delithiated LiCoO₂ lattice.

When the charged state (O1- Li_xCoO_2) was discharged to 3.0 V (ca. 0.43 mol of Li reinserted), (i) some Co-layer distortions still exist along the [001] orientation as shown in Figure 4d and (ii) the Co ion shows a $\alpha\beta\alpha\beta$ -stack model in Figure 4d (O in ABAB-stack model in Figure S11c^{13–16}), which results from the residue Li vacancies ($\text{Li}_{0.931}\square_{0.069}\text{CoO}_2$) in the discharge process. This Co $\alpha\beta\alpha\beta$ -stack model corresponds to O2-LiCoO₂ phase, different from any phase in the presently known phase diagram of O3-LiCoO₂ system (including the stacking of the O1, O3 type, or H1–3 type LiCoO₂⁹). According to the conventional wisdom, O₂-LiCoO₂, which is metastable compared to O₃-LiCoO₂, could be synthesized only by ionic exchanging from NaCoO₂.^{3,4} To the best of our

knowledge, few reports in terms of phase transition between O₂ and O₃ LiCoO₂ phases have been reported; i.e., these two systems are separated once synthesized. Here we directly observed that the O₂-Li_xCoO₂ could be formed in electrochemically cycled O₃-LiCoO₂ electrode by advanced STEM techniques. This discovery makes a connection between the two separated LiCoO₂ systems, at least in nanoscale particles (50 nm) as used in our experiments. It can be deduced that possibly the phase transformation from the O1 type to O2 type is the way of lowest energy cost to bear the stress induced by the Li insertion and also corresponds to the least rearrangement of Co ion in the lattice. Moreover, besides kinks and distortions, the Li-M (transition metal) antisites (rock-salt structure) appeared in the outmost surface region at the end of this electrochemical discharge when charged to 4.5 V (see Li-Co antisites in Figure S14).

Figure 5 shows the possible phase diagram of Li_(1-x)CoO₂ (0 ≤ x ≤ 0.50) based on the above STEM observation and

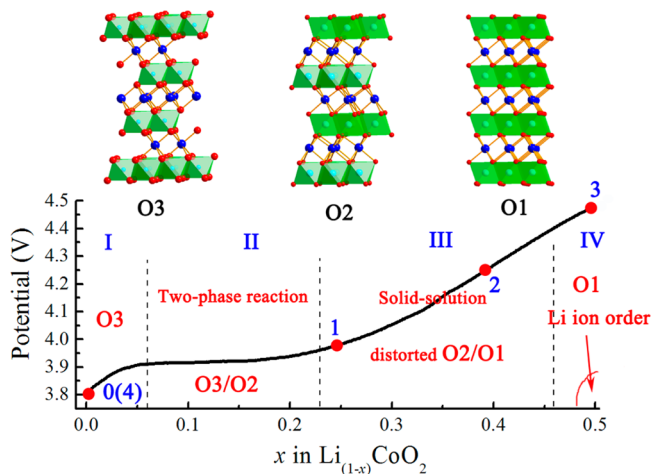


Figure 5. Phase diagram of Li_(1-x)CoO₂ (0 ≤ x ≤ 0.50) nanoparticle. Numerical symbols 0–4 represent the sample points for STEM observation: (0) pristine LiCoO₂, (1) charged to ca. 3.9 V, (2) charged to 4.2 V, (3) charged to 4.5 V, and (4) back to 3.0 V.

analysis. Upon charging, the initial O₃-LiCoO₂ is kept in region I in a solid-solution reaction. Then, a two-phase reaction occurs between O₃- and O₂-type LiCoO₂ in region II. After that, the complex sloped curve in region III can be plausibly ascribed to the solid-solution reactions. However, in this region, the phase transition from the metastable O₂ to O₁ also ends as some small plateaus can be observed in lower charge/discharge rates.^{6,7,10,11} Subsequently in region IV, the O₁-LiCoO₂ is arrived at but with unambiguous distortions. At x close to 0.5, ordered Li ions and Li ion vacancies arrangements are observed as well.

In summary, highly crystallized LiCoO₂ nanoparticles have been synthesized by molten salt method and used for electrochemical and STEM investigations. ABF images of the pristine LiCoO₂ give flawless description of the Li, Co, and O atomic sites in this layered structure. According to the best quality image of atomic-scale LiCoO₂ structure, some new findings are shown:

- (i) The Co-containing (003) layers show a larger planar distance in the surface region than in the bulk. In an electrochemical cycle process, obvious Co (003) layer variations were observed including the regular kinks and

the local distortions. The distortion should be an energetically favorable way to release interior stress induced by Li insertion/extraction.

- (ii) Li ion and Li vacancy exhibit ordered arrangements at x ≈ 0.5 in a Li_xCoO₂ electrode. Simultaneously, staging-like arrangements of the Li ion and Li vacancy were observed perpendicular to (101) plane in O₁-LiCoO₂.
- (iii) The intermediate O₂-LiCoO₂ phase was observed in the electrochemical cycle of the O₃-LiCoO₂ electrode. This discovery makes a connection between the two separated LiCoO₂ phases, i.e., O₂ and O₃ systems.
- (iv) The phase transition mechanism of this nanosized O₃-LiCoO₂ electrode: from O₃ type to O₂ type and then to O₁ type in the charge process; from O₁ type back to O₂ type in the discharge process without Li reversible reinsertion.

Experimental Section. The LiCoO₂ sample was synthesized by a molten salt synthesis method at 700 °C as previously described.³⁹ X-ray powder diffraction (XRD) patterns were recorded in the range of 10°–120° using a Philips X'pert diffractometer with Bragg-Brentano geometry. The measurement was performed in a continuous scan mode, using Cu K α X-ray source and a step of 0.0167°/s. A scanning electron microscope (SEM) (XL 30 S-FEG, FEI Co.) was used to study the sample morphology. Transmission electron microscopy (TEM) studies were carried out on a JEM-2011 electron microscope. Aberration-corrected STEM was performed using a JEOL 2100F (JEOL, Tokyo, Japan) transmission electron microscope equipped with a CEOS (CEOS, Heidelberg, Germany) probe aberration corrector. The attainable spatial resolution of the microscope is 90 pm at an incident angle of 25 mrad. Some raw pictures are dealt with noise reduction by wiener and ABSF filters.⁴⁰

The discharge/charge tests were characterized in a Swagelok-type cell between 3.0 and 4.5 V. Metallic lithium was used as a counter electrode. A polypropylene film (Celgard 2300) was used as a separator. The working electrode was prepared by spreading a slurry of the active material (LiCoO₂), conductive agent (acetylene black: AB), and poly(vinylidene difluoride) (PVDF) in a weight ratio of (LiCoO₂/AB/PVDF) 0.80:0.10:0.10 onto an aluminum foil. The electrolyte solution was 1 M LiPF₆/ethylene carbonate (EC)/dimethyl carbonate (DMC) (EC:DMC = 1:1 by volume). The electrode materials after electrochemical cycle were then carefully washed by DMC solution. The dried electrode materials were then dispersed in ethanol to drop-coat on copper grid for STEM observations. Note that all the operations were performed in an Ar-filled glovebox.

First-principles simulation was performed by VASP.⁴¹ The valence and core interactions were studied by the projector augmented-wave (PAW) method within the generalized gradient approximation plus U (GGA plus U, U_{eff} = 5.0 eV)⁴² with spin polarizations. A 3 × 3 × 1 Monkhorst-Pack k-points grid⁴³ with a Gaussian smearing of 0.1 eV is used in a 2 × 2 × 1 O₂-type LiCoO₂ superlattice. Energy cutoff for plane wave and density were chosen to be 600 eV. The convergence error of the total energy is about 10⁻⁴ eV.

■ ASSOCIATED CONTENT

Supporting Information

XRD pattern, SEM, STEM images, and the schematic representations. This material is available free of charge via the Internet at <http://pubs.acs.org>.

■ AUTHOR INFORMATION

Corresponding Author

*E-mail: yshu@aphy.iphy.ac.cn (Y.-S.H.); lgu@aphy.iphy.ac.cn (L.G.).

Author Contributions

⁸Xia Lu, Yang Sun, and Zelang Jian contribute equally to this work.

Notes

The authors declare no competing financial interest.

■ ACKNOWLEDGMENTS

The authors thank Prof. Xuejie Huang for fruitful discussions. This work was supported by funding from the “863” Project (2009AA033101), “973” Projects (2009CB220104, 2010CB833102), NSFC (50972164, 51222210, 11174334, 11234013), CAS project (KJCX2-YW-W26), and One Hundred Talent Project of the Chinese Academy of Sciences, the WCU (World Class University) program through the Korea Science and Engineering Foundation funded by the Ministry of Education, Science and Technology of Korea (R32-2009-000-20074-0). The calculations were finished at the Virtual Laboratory for Computational Chemistry, Computer NetWork Information Center, Chinese Academy of Sciences.

■ REFERENCES

- (1) Mizushima, K.; Jones, P. C.; Wiseman, P. J.; Goodenough, J. B. *Mater. Res. Bull.* **1980**, *15* (6), 783–789.
- (2) Nagaura, T. 3rd Int. Battery Seminar, Deerfield Beach, FL, 1990.
- (3) Delmas, C.; Braconnier, J. J.; Hagenmuller, P. *Mater. Res. Bull.* **1982**, *17*, 117.
- (4) Carlier, D.; Saadoune, I.; Suard, E.; Croguennec, L.; Ménétrier, M.; Delmas, C. *Solid State Ionics* **2001**, *144*, 263.
- (5) Thomas, M. G. S. R.; Bruce, P. G.; Goodenough, J. B. *Solid State Ionics* **1985**, *17*, 13–19.
- (6) Reimers, J. N.; Dahn, J. R. *J. Electrochem. Soc.* **1992**, *139*, 2091–2097.
- (7) Ohzuku, T.; Ueda, A. *J. Electrochem. Soc.* **1994**, *141*, 2972–2977.
- (8) Wolverton, C.; Zunger, A. *Phys. Rev. Lett.* **1998**, *81*, 606–609.
- (9) Van der Ven, A.; Aydinol, M. K.; Ceder, G.; Kresse, G.; Hafner, J. *Phys. Rev. B* **1998**, *58* (6), 2975–2987.
- (10) Shao-Horn, Y.; Levasseur, S.; Weill, F.; Delmas, C. *J. Electrochem. Soc.* **2003**, *150*, A366–A373.
- (11) Amatucci, G. G.; Tarascon, J. M.; Klein, L. C. *J. Electrochem. Soc.* **1996**, *143*, 1114–1123.
- (12) Liu, L. J.; Chen, L. Q.; Huang, X. J.; Yang, X. Q.; Yoon, W.-S.; Lee, H. S.; McBreen, J. *J. Electrochem. Soc.* **2004**, *151*, A1344–A1351.
- (13) Mendiboure, A.; Delmas, C.; Hagenmuller, P. *Mater. Res. Bull.* **1984**, *19*, 1383–1392.
- (14) Delmas, C.; Braconnier, J. J.; Hagenmuller, P. *Mater. Res. Bull.* **1984**, *17*, 117–123.
- (15) Carlier, D.; Saadoune, I.; Ménétrier, M.; Delmas, C. *J. Electrochem. Soc.* **2002**, *149*, A13410–A1320.
- (16) Carlier, D.; Van der Ven, A.; Delmas, C.; Ceder, G. *Chem. Mater.* **2003**, *15*, 2651–2660.
- (17) Levasseur, S.; Ménétrier, M.; Suard, E.; Delmas, C. *Solid State Ionics* **2000**, *128*, 11–24.
- (18) Chiang, Y. M.; Wang, H. F.; Jang, Y. I. *Chem. Mater.* **2001**, *13*, 53–63.
- (19) Ménétrier, M.; Saadoune, I.; Levasseur, S.; Delmas, C. *J. Mater. Chem.* **1999**, *9*, 1135–1140.
- (20) Marianetti, C. A.; Kotliar, G.; Ceder, G. *Nat. Mater.* **2004**, *3*, 627.
- (21) Shao-Horn, Y.; Croguennec, L.; Delmas, C.; Nelson, E. C.; O’Keefe, M. A. *Nat. Mater.* **2003**, *2*, 464–467.
- (22) Huang, R.; Hitosugi, T.; Findlay, S. D.; Fisher, C. A. J.; Ikuhara, Y. H.; Moriwake, H.; Oki, H.; Ikuhara, Y. *Appl. Phys. Lett.* **2011**, *98*, 051913.
- (23) Huang, R.; Ikuhara, Y. *Curr. Opin. Solid State Mater. Sci.* **2011**, *16*, 31–18.
- (24) Gu, L.; Zhu, C. B.; Li, H.; Yu, Y.; Li, C. L.; Tsukimoto, S.; Maier, J.; Ikuhara, Y. *J. Am. Chem. Soc.* **2011**, *133*, 4661–4663.
- (25) Suo, L. M.; Han, W. Z.; Lu, X.; Gu, L.; Hu, Y.-S.; Li, H.; Chen, D. F.; Chen, L. Q.; Tsukimoto, S.; Ikuhara, Y. *Phys. Chem. Chem. Phys.* **2012**, *14*, 5363–5367.
- (26) Oshima, Y.; Sawada, H.; Hosokawa, F.; Okunishi, E.; Kaneyama, T.; Kondo, Y.; Niitaka, S.; Takagi, H.; Tanishiro, Y.; Takayanagi, K. *J. Electron. Microsc.* **2010**, *59*, 457–461.
- (27) Chung, S. Y.; Choi, S. Y.; Yamamoto, T.; Ikuhara, Y. *Phys. Rev. Lett.* **2008**, *100*, 125502.
- (28) Huang, R.; Ikuhara, Y. H.; Mizoguchi, T.; Findlay, S. D.; Kuwabara, A.; Fisher, C. A. J.; Moriwake, H.; Oki, H.; Hirayama, T.; Ikuhara, Y. *Angew. Chem., Int. Ed.* **2011**, *50*, 3053–3057.
- (29) Lu, X.; Jian, Z. L.; Fang, Z.; Gu, L.; Hu, Y. S.; Chen, W.; Wang, Z. X.; Chen, L. Q. *Energy Environ. Sci.* **2011**, *4*, 2638–2644.
- (30) Lu, X.; Zhao, L.; He, X. Q.; Xiao, R. J.; Gu, L.; Hu, Y.-S.; Li, H.; Wang, Z. X.; Duan, X. F.; Chen, L. Q.; Maier, J.; Ikuhara, Y. *Adv. Mater.* **2012**, *24*, 3233–3238.
- (31) Pennycook, S. J.; Jesson, D. E. *Scanning Transmission Electron Microscopy: Imaging and Analysis*; Springer: Berlin, 2011.
- (32) Pennycook, S. J.; Jesson, D. E. *Phys. Rev. Lett.* **1990**, *64*, 938.
- (33) Findlay, S. D.; Saito, T.; Shibata, N.; Sato, Y.; Matsuda, J.; Asano, K.; Akiba, E.; Hirayama, T.; Ikuhara, Y. *Appl. Phys. Express* **2010**, *3*, 116603.
- (34) Ohzuku, T.; Ueda, A.; Nagayama, M.; Iwakoshi, Y.; Komori, H. *Electrochim. Acta* **1993**, *38*, 1159.
- (35) Findlay, S. D.; Shibata, N.; Sawada, H.; Okunishi, E.; Kondo, Y.; Yamamoto, T.; Ikuhara, Y. *Appl. Phys. Lett.* **2009**, *95*, 191913.
- (36) Findlay, S. D.; Shibata, N.; Sawada, H.; Okunishi, E.; Kondo, Y.; Ikuhara, Y. *Ultramicroscopy* **2010**, *110*, 903.
- (37) Van Aert, S.; Batenburg, K. J.; Rossell, M. D.; Erni, R.; Van Tendeloo, G. *Nature* **2011**, *470*, 374–377.
- (38) Okubo, M.; Hosono, E.; Kim, J.; Enomoto, M.; Kojima, N.; Kudo, T.; Zhou, H. S.; Honma, I. *J. Am. Chem. Soc.* **2007**, *129*, 7444–7452.
- (39) Liang, H. Y.; Qiu, X.; Chen, H.; He, Z.; Zhu, W.; Chen, L. Q. *Electrochim. Commun.* **2004**, *6*, 789.
- (40) Killias, R. J. *Microsc.* **1998**, *190*, 45.
- (41) Kresse, G.; Furthmüller, J. *Phys. Rev. B* **1996**, *54*, 11169.
- (42) Anisimov, V. I.; Aryasetiawan, F.; Liechtenstein, A. I. *J. Phys.: Condens. Matter* **1997**, *9*, 767.
- (43) Monkhorst, H. J.; Pack, J. D. *Phys. Rev. B* **1976**, *13*, 5188.